JOURNAL OF SOLID STATE CHEMISTRY **131,** 379–386 (1997)
ARTICLE NO. SC977405

Structure and Properties of the New Phosphides $M_2M'P$ (M = Zr, Hf; M' = Co, Ni) and Their Relations to ZrNi and HfNi

Holger Kleinke and Hugo F. Franzen

Ames Laboratory — DOE, Iowa State University, Ames, Iowa 50011

Received December 13, 1996; in revised form March 28, 1997; accepted April 2, 1997

The isostructural title compounds can be obtained by arc-melting of cold-pressed mixtures of MP, M, and M' in the ratio 1:1:1 (M = Zr, Hf; M' = Co, Ni). Their crystal structure (space group $P2_1/m$, No. 11, $Z = 2$) can be regarded as a new superstructure of the CrB structure type. Thus, the structure of M_2NiP can be derived formally from ZrNi or HfNi (both CrB type) by replacing every second Ni atom by P in such a way that P–P contacts are minimized. Condensed channels formed by zirconium and hafnium, respectively, build up an extended early-transition-metal framework. The late-transition-metal atoms and P are situated in singly capped trigonal prisms of the M sublattice, forming –Ni–P– zigzag chains. The expectation of metallic properties is confirmed by Extended Hückel calculations and experimentally observed Pauli paramagnetism. The differences between Co and Ni on the one hand and between Zr and Hf on the other hand are discussed, as well as the changes from MNi to M_2NiP. © 1997 Academic Press

INTRODUCTION

Within the last 12 years, several refractory metal-rich ternary and higher pnictides and chalcogenides consisting of an early-transition-metal atom and a late-transition-metal atom have been uncovered. All their crystal structures contain 3D extended early-transition-metal substructures with the late-transition-metal atoms as interstitials in one-, two-, or three-capped trigonal prisms. So far, the nonmetal atoms among the chalcogenides, i.e., in $Hf_5M'Te_3$ and $Hf_8M'Te_6$ (M' = Mn, Fe) (1, 2), $Nb_9Ni_{2-x}S_{3+x}$ (3), $Ta_9M'_2S_6$ (M' = Fe, Co, Ni) (4, 5), $Ta_{11}M'_2Se_8$ (M' = Fe, Co, Ni) (6), and Ta_8NiSe_8 (7), sheathe the metal sublattice, surrounding otherwise empty channels. As for the phosphides $Zr_9M'_2P_4$ (M' = Co, Ni) (8), $Hf_5Co_{1+x}P_{3-x}$ (9), and $Hf_5Ni_{1+x}P_3$ (10), the nonmetal atoms are located in one-, two-, or three-capped trigonal prismatic voids of the Zr and Hf sublattice, respectively. The first arsenide in this class, Zr_6CoAs_2 (11), occurs in an ordered variant of the Fe_2P structure type, isotypic with $Zr_6M'Te_2$ (M' = Mn, Fe, Co, Ni, Ru, Pt) (12), and can thus be regarded as the missing link between the structures of these chalcogenides and pnictides. However, the similar coordination chemistry and sizes of the late-transition-metal atoms and phosphorus led to mixed Co/P occupancy of one P position in $Hf_5Co_{1+x}P_{3-x}$, occurring with a partial reduction of the Hf sublattice compared to Hf_5CoP_3 (13). The idea of replacing each second Ni atom in HfNi (14) yielded the expected structure of Hf_2NiP (15), which is a part of the $Hf_5M'P_3$ structure. Although HfCo crystallizes in the CsCl type (14), Hf_2CoP could also be prepared. Somewhat surprising was the successful exchange of Hf with Zr, leading to the synthesis of Zr_2CoP and Zr_2NiP, which are the first examples of isotypic Zr and Hf compounds in the class of compounds discussed here, including the tellurides $Hf_8M'Te_6$ and $Hf_5M'Te_3$. In addition, there are also no Nb sulfides or selenides isotypic to $Ta_9M'_2S_6$, $Ta_{11}M'_2Se_8$, and Ta_8NiSe_8, and $Nb_9Ni_{2-x}S_{3+x}$ has no Ta counterpart.

After a short communication about the synthesis of Hf_2NiP (15), we describe here in detail the crystal structure of Hf_2CoP, Zr_2CoP, and Zr_2NiP, as well as their electronic structures and properties. Since all four isotypic phosphides $M_2M'P$ with M = Zr, Hf; M' = Co, Ni are known, one can investigate the changes in structure and bonding which originate from replacing Co by Ni and Hf by Zr via the scales of Mulliken overlap populations (MOP) and Pauling bond orders (PBO). Also discussed here are the differences between the intermetallics ZrNi and HfNi and the phosphides Zr_2NiP and Hf_2NiP.

EXPERIMENTAL

Synthesis

The starting materials are the monophosphides ZrP and HfP, and the metals Zr (ALFA AESAR, powder, $-20 + 60$ mesh, purity 99.7% (Hf impurity: 97 ppm)), Hf (ALFA AESAR, powder, -325 mesh, purity 99.6% (containing 2–3.5% Zr)), Co (ALFA AESAR, powder, $-50 + 150$ mesh, 99.9%), and Ni (FISHER, purified powder). For the preparation of the monophosphides, 15 mmol of Zr and Hf, respectively, and 15 mmol P (ALFA

0022-4596/97 $25.00

AESAR, powder, −100 mesh, red amorphous, 99%) were filled into a silica tube. After the silica tube was sealed under a vacuum of 10^{-2} bar, the tube was placed in a resistance furnace and then slowly heated to 500°C. After three days of annealing at 500°C the temperature was increased to 800°C and held there for 3 more days. The powder diagrams of the products experimentally obtained contained only the reflections of ZrP and HfP, respectively. For the synthesis of the title compounds $M_2M'P$ mixtures of 1.25 mmol MP, 1.25 mmol M, and 1.25 mmol M', corresponding to the stoichiometric ratio $M:M':P \equiv 2:1:1$, were thoroughly mixed and then cold-pressed into pellets. These pellets were arc-melted twice under an argon flow with inversion of the sample after the first melt. Single crystals were obtained after annealing in an induction furnace at 1400°C under dynamic vacuum (10^{-6} bar) over periods of 5–7 h. To obtain more homogeneous products, samples of Zr_2NiP and Hf_2NiP were annealed in Ta tubes over a period of 6 days at 1400°C.

Structure Determinations

In all four cases, small needle-like single crystals were selected for data collection, which was performed using an automatic four-circle Rigaku AFC6R diffractometer with graphite monochromatic Mo$K\alpha$ radiation and a 12 KW rotating anode. The orientation matrices and cell constants were obtained after least-squares refinement of at least 15 carefully refined reflections in the range $13.5° < 2\theta < 22.5°$. The observed intensities were corrected for Lorentz polarization. The structure of Hf_2NiP was solved in space group $P2_1/m$, which is consistent with the observed extinction of $k = 2n + 1$ for all $0k0$ reflections. Final refinements with anisotropic temperature factors for the metal positions, carried out against F^2, yielded reasonable residual factors. The atomic positions of Hf_2NiP were used as a starting model for Zr_2CoP, Zr_2NiP, and Hf_2CoP. More detailed information can be found in Table 1. Atomic positions and equivalent temperature factors are given in Table 2, interatomic distances in Table 3.

Magnetic Measurements

Magnetic data were obtained for Zr_2NiP and Hf_2NiP from bulk samples of mass 32.0 mg and 112.7 mg. Temperature dependent measurements of the magnetic susceptibilities were made at 3 T in the temperature range 5–300 K on a Quantum Design MPMS SQUID magnetometer. The data were corrected for the diamagnetic atom cores.

RESULTS AND DISCUSSION

As described earlier, the most striking motifs of the crystal structure of $Hf_5Co_{1+x}P_{3-x}$ are the channels formed by Hf atoms, filled with an infinite –Co–P– chain (9). The structures of the intermetallics ZrNi and HfNi (14) consist of very similar channels containing infinite –Ni–Ni– chains, as shown in Fig. 1. Replacing every second Ni atom in ZrNi leads formally to the structure of Zr_2NiP. As can be seen in Fig. 2, the orientation of the –Ni–P– chain is inverted from one channel to the next along the crystallographic c axis, related to an inversion center. The main driving force for

TABLE 1
Selected Crystallographic Data for $M_2M'P$ (M = Zr, Hf; M' = Co, Ni)

Empirical formula	Zr_2CoP	Zr_2NiP	Hf_2CoP	Hf_2NiP
Space group	$P2_1/m$ (No. 11)	$P2_1/m$ (No. 11)	$P2_1/m$ (No. 11)	$P2_1/m$ (No. 11)
Z	2	2	2	2
Unit cell dimensions				
a	5.275(1) Å	5.264(2) Å	5.2245(8) Å	5.2259(9) Å
b	3.7158(5) Å	3.676(1) Å	3.6786(6) Å	3.6567(8) Å
c	7.148(3) Å	7.293(2) Å	7.0671(8) Å	7.192(1) Å
β	109.82(2)°	110.24(2)°	109.75(1)°	110.12(1)°
V	131.8(1) Å^3	132.4(1) Å^3	127.83(3) Å^3	129.05(8) Å^3
Calculated density [g/cm^3]	6.862	6.825	11.609	11.49
Absorption coefficient [cm^{-1}]	141.05	149.34	869.73	870.7
F(000)	244	246	372	374
Scan mode, scan width	ω–2θ, $(1.50 + 0.34\tan\theta)°$	ω–2θ, $(1.60 + 0.34\tan\theta)°$	ω–2θ, $(1.70 + 0.34\tan\theta)°$	ω–2θ, $(1.30 + 0.34\tan\theta)°$
Scan speed	2.0°/min (in ω, max. 3 rescans)	4.0°/min (in ω, max. 3 rescans)	4.0°/min (in ω, max. 3 rescans)	2.0°/min (in ω, max. 3 rescans)
Range of 2θ	3°–54°	3°–70°	3°–70°	3°–70°
No. of measured reflections	952	1268	1229	1289
No. of independent reflections	341 ($R_{int} = 0.040$)	659 ($R_{int} = 0.091$)	640 ($R_{int} = 0.056$)	647 ($R_{int} = 0.088$)
No. of observed reflections ($I > 3.0\sigma(I)$)	127	206	279	184
No. of parameters refined	23	23	23	23
Max., min. res. electron density	0.88, $-0.75\ e^-$/Å^3	1.53, $-1.75\ e^-$/Å^3	2.33, $-4.28\ e^-$/Å^3	4.41, $-4.33\ e^-$/Å^3
$R(F)$, $R(F^2)$, $R_w(F^2)$, goodness of fit	0.014, 0.022. 0.027, 1.15	0.026, 0.042, 0.052, 1.20	0.022, 0.038, 0.045, 1.37	0.038, 0.065, 0.070, 1.08
Extinction coefficient	0	2.953×10^{-7}	7.403×10^{-7}	1.104×10^{-7}
Absorption correction	DIFABS	Ψ scan	Ψ scan	DIFABS

TABLE 2
Atomic Positions and Equivalent Temperature Factors

Atom	x	y	z	$B_{eq}/Å^2$
		(a) Zr_2CoP		
Zr1	0.8025(3)	1/4	0.0765(3)	0.26(4)
Zr2	0.7828(3)	1/4	0.5698(3)	0.44(1)
Co	0.3506(4)	1/4	0.7124(3)	0.63(6)
P	0.3464(8)	1/4	0.2117(6)	0.73(7)
		(b) Zr_2NiP		
Zr1	0.7952(5)	1/4	0.0762(3)	0.41(4)
Zr2	0.7882(5)	1/4	0.5672(3)	0.47(4)
Ni	0.3468(6)	1/4	0.7056(4)	0.77(6)
P	0.355(1)	1/4	0.2251(7)	0.56(7)
		(c) Hf_2CoP		
Hf1	0.7982(2)	1/4	0.0779(2)	0.33(2)
Hf2	0.7925(2)	1/4	0.5696(2)	0.51(2)
Co	0.3481(6)	1/4	0.7054(5)	0.39(6)
P	0.351(1)	1/4	0.226(1)	0.55(8)
		(d) Hf_2NiP		
Hf1	0.7959(6)	1/4	0.0824(4)	0.40(5)
Hf2	0.7916(6)	1/4	0.5642(4)	0.40(5)
Ni	0.346(1)	1/4	0.704(1)	0.5(2)
P	0.358(3)	1/4	0.227(2)	0.2(2)

this ordering is most likely the minimizing of anti-bonding P–P contacts.

However, the alternation of the –Ni–P– chains comes along with a symmetry reduction to the monoclinic system. It also leads to a doubling of the primitive cell of ZrNi, the unit cell of Zr_2NiP can thus be considered a $2c$ superstructure of ZrNi. The matrix for the transformation of the centered cell of ZrNi to Zr_2NiP is $(0.5, 0.5, 0 / 0, 0, 1/\bar{2}, 0, 0)$. This transformation yields lattice constants for the transformed ZrNi cell of $a = 5.230$ Å, $b = 4.101$ Å, $c = 6.536$ Å, $\beta = 108.21°$. The a axis and β are almost equal to those of Zr_2NiP, whereas b is more than 10% longer and c more than 10% shorter, yielding almost identical cell volumes. These differences occur with significant changes in the Zr substructure as well as in the –Ni–P– chain.

The coordination spheres of Ni and P in the structure of Zr_2NiP are very similar (Fig. 3). Ni is surrounded by six Zr atoms, forming a trigonal prism. One rectangular face of the prism is capped by a Zr atom ($\bar{d}_{Ni-Zr} = 2.736$ Å) and the two remaining faces by P atoms ($d_{Ni-P} = 2.356(3)$ Å). On the other hand, the P atom is also situated in a trigonal Zr_6 prism, which is capped by one Zr atom ($\bar{d}_{P-Zr} = 2.743$ Å) and two Ni atoms. All together, both coordinations may be considered as tetrakaidecahedra which are very common polyhedra in metal-rich phosphides and chalcogenides. Usually, the mean distances between the early- and late-transition-metal atoms are shorter than those between P and the early-transition metal, although the Pauling radius of P (1.10 Å) is somewhat smaller than the radii of Co (1.162 Å) and Ni (1.154 Å) (16). The longer M–P bonds indicate a more negative charge of P compared to Co or Ni. Examples with M' and P in the centers of capped trigonal M prisms are Hf_2CoP ($\bar{d}_{P-Hf} = 2.711$ Å, $\bar{d}_{Co-Hf} = 2.704$ Å), Hf_2NiP ($\bar{d}_{P-Hf} = 2.733$ Å, $\bar{d}_{Ni-Hf} = 2.704$ Å), $Hf_5Co_{1+x}P_{3-x}$ ($\bar{d}_{P-Hf} = 2.691$ Å, $\bar{d}_{Co-Hf} = 2.677$ Å), and $Zr_9Ni_2P_4$ ($\bar{d}_{P-Zr} = 2.759$ Å, $\bar{d}_{Ni-Zr} = 2.732$ Å). The only exception so far is Zr_2CoP with $\bar{d}_{P-Zr} = 2.725$ Å $< \bar{d}_{Co-Zr} = 2.738$ Å. In all cases, however, the P–M and M'–M distances are only slightly longer than the sums of the radii, indicating bonding character.

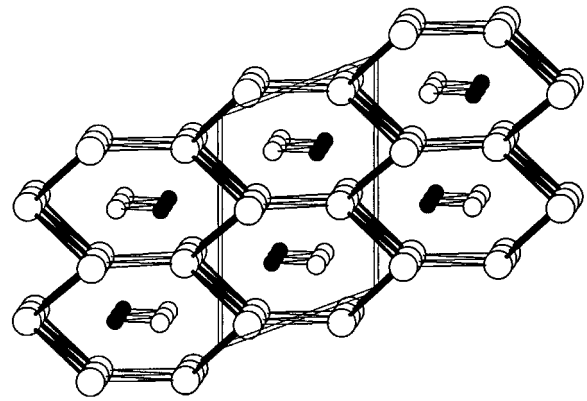

FIG. 2. Projection of the structure of Zr_2NiP in a projection along [010]. Vertical: c axis. Small, black circles: Ni; medium, white circles: P; large, white circles: Zr.

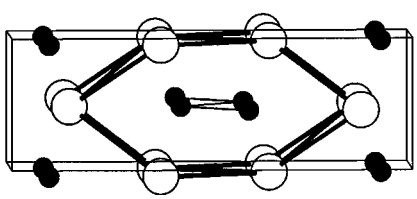

FIG. 1. Projection of the structure of ZrNi in a projection along [001]. Vertical: a axis. Small, black circles: Ni; large, white circles: Zr.

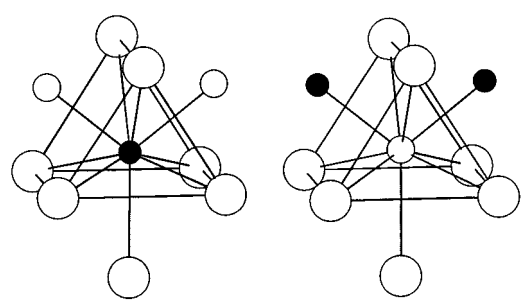

FIG. 3. Coordination spheres around Ni (left) and P (right) in the structure of Zr_2NiP.

TABLE 3
Selected Interatomic Distances [Å] for $M_2M'P$

Central atom	Neighbors	Distance in Zr_2CoP	Distance in Zr_2NiP	Distance in Hf_2CoP	Distance in Hf_2NiP
*M*1	2 *M*1	3.246(3)	3.304(5)	3.257(2)	3.322(5)
*M*1	2 *M*1	3.531(3)	3.447(4)	3.463(2)	3.434(5)
*M*1	2 *M*1	3.7158(5)	3.676(1)	3.6786(7)	3.6567(8)
*M*1	2 *M*2	3.298(1)	3.309(2)	3.2496(7)	3.268(2)
*M*1	*M*2	3.562(4)	3.609(4)	3.485(2)	3.473(5)
*M*1	*M*2	3.588(4)	3.685(4)	3.583(2)	3.719(5)
*M*1	2 *M*′	2.685(2)	2.701(3)	2.665(3)	2.653(6)
*M*1	*M*′	2.872(3)	2.909(3)	2.877(3)	2.922(7)
*M*1	2 P	2.686(3)	2.762(4)	2.735(5)	2.78(1)
*M*1	P	2.699(5)	2.764(6)	2.717(6)	2.76(1)
*M*1	P	2.881(5)	2.881(7)	2.869(7)	2.82(2)
*M*2	2 *M*1	3.298(1)	3.309(2)	3.2496(7)	3.268(2)
*M*2	*M*1	3.562(4)	3.609(4)	3.485(2)	3.473(5)
*M*2	*M*1	3.588(4)	3.685(4)	3.583(2)	3.719(5)
*M*2	2 *M*2	3.353(3)	3.305(5)	3.239(2)	3.213(5)
*M*2	2 *M*2	3.366(3)	3.389(5)	3.415(2)	3.398(5)
*M*2	2 *M*2	3.7158(5)	3.676(1)	3.6786(7)	3.6567(8)
*M*2	2 *M*′	2.656(2)	2.629(2)	2.595(2)	2.573(5)
*M*2	*M*′	2.795(3)	2.759(4)	2.732(3)	2.719(7)
*M*2	*M*′	2.818(3)	2.827(4)	2.797(4)	2.836(9)
*M*2	2 P	2.661(4)	2.641(5)	2.598(5)	2.65(1)
*M*2	P	2.803(4)	2.747(5)	2.726(6)	2.69(1)
M′	2 *M*1	2.685(2)	2.701(3)	2.665(3)	2.653(6)
M′	*M*1	2.872(3)	2.909(3)	2.877(3)	2.922(7)
M′	2 *M*2	2.656(2)	2.629(2)	2.595(2)	2.573(5)
M′	*M*2	2.795(3)	2.759(4)	2.732(3)	2.719(7)
M′	*M*2	2.818(3)	2.827(4)	2.797(4)	2.836(9)
M′	2 *M*′	3.7158(5)	3.676(1)	3.6786(7)	3.6567(8)
M′	2 P	2.390(2)	2.356(3)	2.362(3)	2.337(7)

Significant homoatomic interactions occur only within the *M* sublattice. The shortest Zr–Zr bonds of ca. 3.3 Å form puckered Zr layers along (011), as emphasized with bold lines in Fig. 2. These layers are interconnected via longer Zr–Zr interactions of 3.4 Å (thinner lines in Fig. 2) to a three-dimensional Zr sublattice. The Zr–Zr separations parallel to [001] and [010] (> 3.59 Å, not shown in Fig. 2) are significantly longer, in contrast to the structure of ZrNi. In ZrNi, the shortest Zr–Zr bonds ($d_{Zr-Zr} = 3.268$ Å) are parallel to the crystallographic *a* axis, which corresponds to the *c* axis of Zr_2NiP. The other Zr–Zr interactions in ZrNi are significantly longer (>3.42 Å). Also, the Ni–Ni contacts are much longer than the Ni–P bonds in Zr_2NiP (2.616 Å vs. 2.356(3) Å). Thus, the main driving force for the structural differences is most likely to be the formation of strong bonding Ni–P interactions, whereas the Ni–Ni interactions in ZrNi might have only weak bonding character.

In order to get more information about bonding in $M_2M'P$ and *M*Ni, we calculated the Pauling bond orders (using Pauling's equation $d(n) = d(1) - 0.6 \log n$, with $n =$ bond order, $r_{Zr} = 1.454$ Å, and $r_{Hf} = 1.442$ Å) for these six compounds as well as the electronic structures, using the extended Hückel approximation (17, 18). The parameters for Zr and Hf were taken from solid state charge iterations, performed on Zr_7P_4 and Hf_7P_4 (19–21), the P parameters

TABLE 4
Parameters Used for the Extended Hückel Calculations

Orbital	H_{ii}/eV	V_1	c_1	V_2	c_2
Zr, 5*s*	−8.93	1.82			
Zr, 5*p*	−5.29	1.78			
Zr, 4*d*	−9.24	3.84	0.6207	1.505	0.5793
Hf, 6*s*	−8.58	2.21			
Hf, 6*p*	−4.98	2.17			
Hf, 5*d*	−8.71	4.36	0.7145	1.709	0.5458
Co, 4*s*	−8.36[a]/−8.05[b]	2.00			
Co, 4*p*	−4.26[a]/−4.01[b]	2.00			
Co, 3*d*	−10.37[a]/−9.87[b]	5.55	0.5679	2.100	0.6059
Ni, 4*s*	−8.56[a]/−8.25[b]	1.93			
Ni, 4*p*	−4.21[a]/−3.98[b]	1.93			
Ni, 3*d*	−11.00[a]/−10.51[b]	5.75	0.5862	2.200	0.5845
P, 3*s*	−18.60	1.88			
P, 3*p*	−12.50	1.63			

[a] Ionization potentials used for Zr compounds.
[b] Ionization potentials used for Hf compounds.

TABLE 5
Mulliken Overlap Populations (MOP) for Selected Interatomic Interactions for M_2M'P

Central atom	Neighbors	MOP in Zr_2CoP	MOP in Zr_2NiP	MOP in Hf_2CoP	MOP in Hf_2NiP
*M*1	2 *M*1	0.085	0.087	0.083	0.081
*M*1	2 *M*1	0.041	0.058	0.046	0.053
*M*1	2 *M*1	0.052	0.066	0.061	0.066
*M*1	2 *M*2	0.100	0.103	0.101	0.104
*M*1	*M*2	0.129	0.119	0.133	0.146
*M*1	*M*2	0.029	0.026	0.027	0.025
*M*1	2 *M*′	0.173	0.141	0.174	0.146
*M*1	*M*′	0.045	0.032	0.043	0.029
*M*1	2 P	0.186	0.167	0.165	0.159
*M*1	P	0.177	0.162	0.164	0.158
*M*1	P	0.254	0.260	0.244	0.272
*M*2	2 *M*1	0.100	0.103	0.101	0.104
*M*2	*M*1	0.129	0.119	0.133	0.146
*M*2	*M*1	0.029	0.028	0.027	0.025
*M*2	2 *M*2	0.122	0.134	0.130	0.114
*M*2	2 *M*2	0.074	0.073	0.049	0.039
*M*2	2 *M*2	0.048	0.058	0.044	0.042
*M*2	2 *M*′	0.180	0.151	0.186	0.156
*M*2	*M*′	0.126	0.117	0.141	0.115
*M*2	*M*′	0.101	0.065	0.083	0.054
*M*2	2 P	0.278	0.291	0.295	0.277
*M*2	P	0.279	0.312	0.300	0.330
M′	2 *M*1	0.173	0.141	0.174	0.146
M′	*M*1	0.045	0.032	0.043	0.029
M′	2 *M*2	0.180	0.151	0.186	0.156
M′	*M*2	0.126	0.117	0.141	0.115
M′	*M*2	0.101	0.065	0.083	0.054
M′	2 *M*′	−0.004	−0.004	−0.005	−0.004
M′	2 P	0.120	0.130	0.123	0.129
M′	P	−0.012	−0.013	−0.017	−0.016
M′	P	−0.006	−0.004	−0.005	−0.005

from standard sources (22). The Co and Ni parameters for the Zr compounds were obtained from charge iteration on Zr_2CoP and Zr_2NiP, respectively; those for the Hf compounds from charge iteration on Hf_2CoP and Hf_2NiP, respectively. A list of the Hückel parameters is given in Table 4. The Mulliken overlap populations (MOP) for M_2M'P can be found in Table 5, and the corresponding values for ZrNi and HfNi in Table 6.

TABLE 6
Interactions in ZrNi and HfNi

Central atom	Neighbors	length/Å in ZrNi	MOP in ZrNi	length/Å in HfNi	MOP in HfNi
M	2 *M*	3.268	0.168	3.220	0.178
M	4 *M*	3.425	0.133	3.403	0.131
M	2 *M*	3.442	0.069	3.422	0.069
M	2 *M*	4.101	0.032	4.120	0.029
Sum			1.070		1.076
M	4 Ni	2.683	0.129	2.675	0.129
M	2 Ni	2.736	0.092	2.701	0.095
M	1 Ni	2.774	0.201	2.742	0.211
Sum			0.901		0.917
Ni	2 Ni	2.616	0.018	2.611	0.018
Ni	2 Ni	3.268	0.001	3.220	0.002
Ni	2 Ni	4.101	−0.003	4.120	−0.003
Sum			0.032		0.034

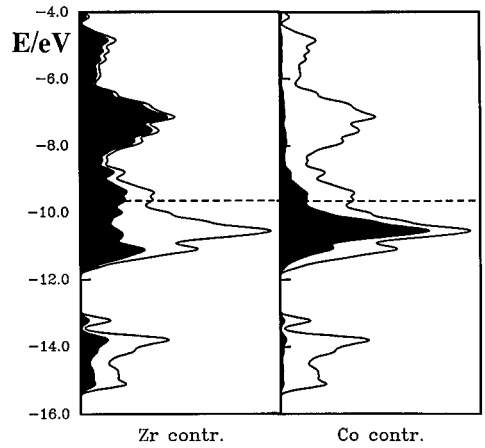

FIG. 4. Density of states for Zr_2CoP. Dashed line: Fermi level. Left: Zr; right: Co contributions emphasized.

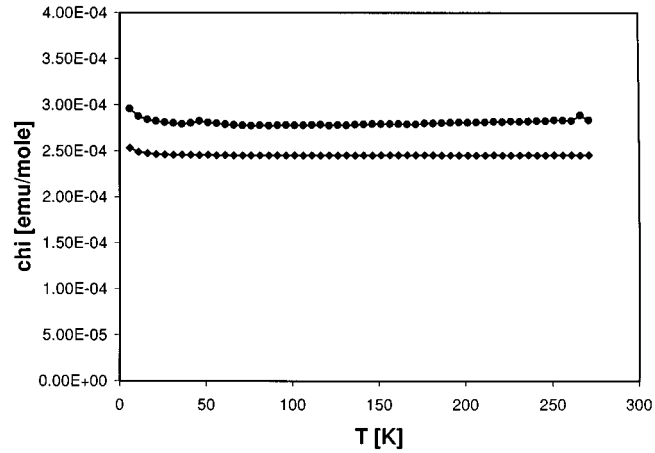

FIG. 6. Temperature dependence of the magnetic susceptibilities for Zr_2NiP (circles) and Hf_2NiP (diamonds).

All four $M_2M'P$ compounds show a significant number of states at the Fermi level. Under consideration of the three-dimensional M framework, 3D metallic behavior, i.e., metallic conductivity and Pauli paramagnetism, can be expected. The P states are found at low energies (below -13 eV), but strong covalent mixing with the M and M' states leads to significant M and M' contributions at these low energies. The d states of Co are localized in a broad peak around -10.5 eV for Zr_2CoP, as shown in Fig. 4, whereas the corresponding Ni peak is narrower for Zr_2NiP (Fig. 5). It turns out that in contrast to the d states of Co, the Ni d states are more or less completely filled. In both cases the d states of Zr predominate at the Fermi level, but the iron-group metal atom has a higher contribution at the Fermi level in case of Zr_2CoP.

The only significant difference between the density of states (DOS) of $Zr_2M'P$ and $Hf_2M'P$ is that the Zr states are slightly shifted to lower energy, due to the lower ionization potential of Zr. Due to the lower Fermi level, the Zr compounds have more contributions of the d states of M' at the Fermi level, and thus more states at the Fermi level. The experimentally observed weak, almost temperature independent Pauli paramagnetism, being proportional to the number of states at the Fermi level, is thus higher for Zr_2NiP than for Hf_2NiP (Fig. 6).

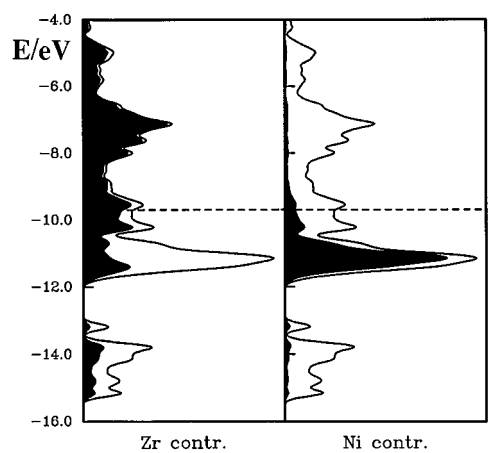

FIG. 5. Density of states for Zr_2NiP. Dashed line: Fermi level. Left: Zr; right: Ni contributions emphasized.

However, the M–P bonds in all $M_2M'P$ show the largest overlap populations, ranging from 0.158 to 0.330. These correspond to strong bonding interactions, as expected between the most electropositive (M) and the most electronegative (P) elements of these compounds. As discussed earlier, the M'–P bonds have significant positive overlap populations, too, with bond orders between 0.61 and 0.73. On the other hand, the (longer) Ni–Ni interactions in MNi have only very small overlap populations of 0.018. Thus, the suggestion of the formation of M'–P bonding interactions as a driving force for the structural changes from MNi to M_2NiP is confirmed by the calculations of the electronic structures.

The M–M' interactions in $M_2M'P$, as well as in MNi, also have bonding character, corresponding to Lewis' acid/base concept, considering the electron-poor M atoms as acid and the electron-rich M' atoms as base. The MOPs in $M_2M'P$, varying from 0.029 (for the longest M–M' contact) to 0.186, are comparable to the mean MOPs of the Zr–Ni bonds in $Zr_9Ni_2P_4$ of 0.113 and of the Zr–Fe bonds in $Zr_6I_{14}Fe$ of 0.16, where bonding character is indicated by MO calculations (23). Since P is more electron deficient than Ni, it attracts more electron density, leading to lower M–Ni overlap populations in M_2NiP than in MNi. Probably for the same reason, the MOPs for the M–M interactions are smaller in M_2NiP than in MNi. However, in all cases the expectation of bonding character of the M–M interactions <3.5 Å is confirmed by the positive overlap populations.

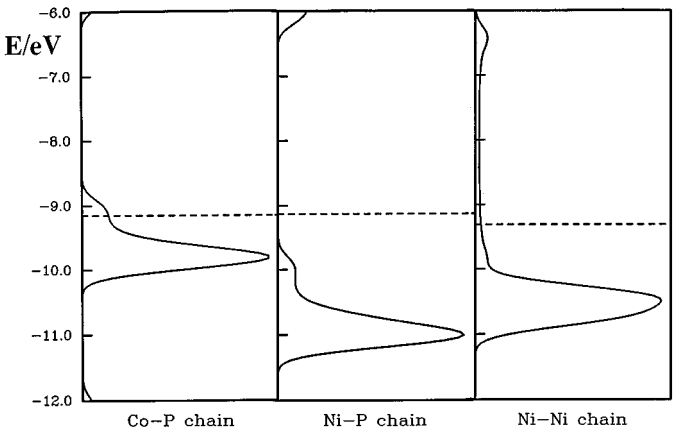

FIG. 7. Density of states for the different chains. Dashed line: Fermi levels of the parent compounds. Left: –Co–P– chain of Hf_2CoP; middle: –Ni–P– chain of Hf_2NiP; right: –Ni–Ni– chain of HfNi.

It turns out that the shortest M–M bonds of ca. 3.3 Å are not the strongest: the bonds parallel to the c axis which are close to M' have in all four M_2M'P structures the highest overlap populations (ranging from 0.119 in Zr_2NiP to 0.146 in Hf_2NiP), although their lengths are much longer (between 3.473(5) Å and 3.609(4) Å). These bonds alternate along c with slightly longer (between 3.588(4) Å and 3.719(5) Å), but much weaker M–M interactions (MOP < 0.03). As mentioned previously, the corresponding distances in the structure of the intermetallics are there the shortest, and they have the highest overlap populations (0.168 in ZrNi and 0.178 in HfNi).

Altogether, the M–M and M–M' overlap populations are considerably higher for the intermetallics MNi, compared to M_2NiP. This is most likely caused by the more oxidizing nature of P, in comparison to Ni. Electronic calculations of the –Ni–Ni– chain of HfNi and of the –Ni–P– chain of Hf_2NiP reveal another significant difference between HfNi and Hf_2NiP: whereas the Ni sublattice of HfNi provides some states in the region between -12 and -6 eV, only the –Ni–P– chain shows a band gap at the Fermi level of the parent structure Hf_2NiP (Fig. 7). Exactly 18 electrons fill the orbitals below this gap, corresponding to closed shells, i.e., the d states of Ni and the s and p states of P. On the other hand, the electron deficient –Co–P– chain also has metallic character, indicating that the d states of Co are not completely filled.

This electron deficiency comes along with some differences in bonding between M_2CoP and M_2NiP. In general, a replacement of Ni by Co yields a lower valence electron concentration (vec), energetically higher lying d states, and larger d orbitals. As can be seen in Figs. 8 and 9, the Zr–M' interactions are almost optimized for Zr_2CoP as well as for Zr_2NiP, so that the vec might not play a significant role for the Zr–M' interactions. The overlap populations for the

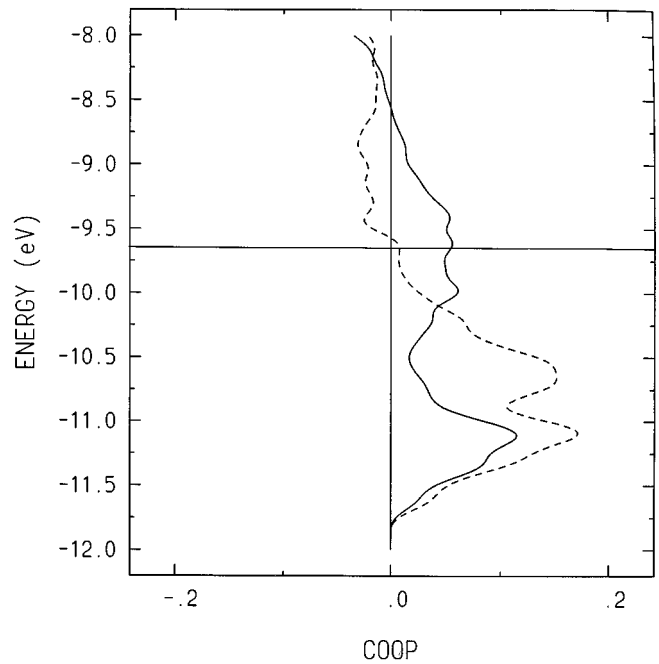

FIG. 8. Crystal orbital overlap populations for Zr_2CoP. Solid, horizontal line: Fermi level. Solid line: Zr–Zr; dashed line: Zr–Co interactions. Left part of the diagram: antibonding interactions ($-$), right: bonding ($+$).

Zr–Co interactions are even higher than for Zr–Ni, probably because of the greater extension of the d states of Co and the more electron deficient character of Co. The Zr–Zr bonds have smaller MOPs in the case of Zr_2CoP, most

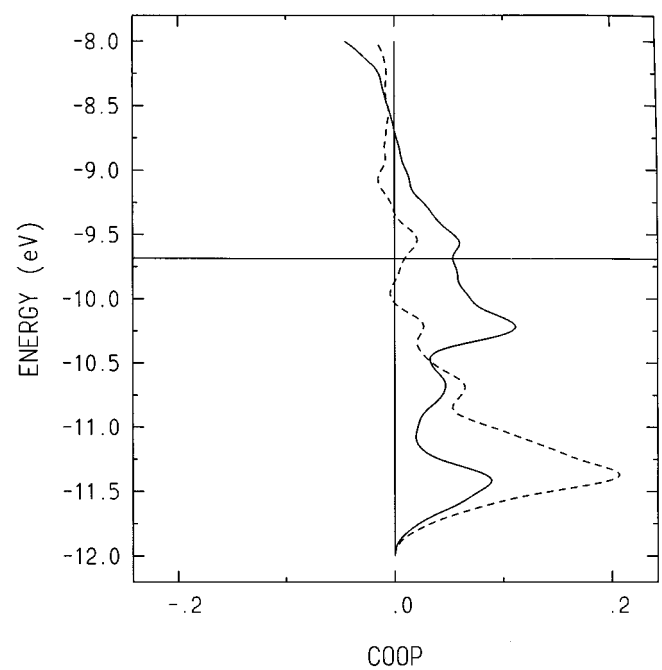

FIG. 9. Crystal orbital overlap populations for Zr_2NiP. Solid, horizontal line: Fermi level. Solid line: Zr–Zr; dashed line: Zr–Ni interactions. Left part of the diagram: antibonding interactions ($-$), right: bonding ($+$).

likely because of the lower vec. However, increasing the vec in Zr_2NiP, e.g., by a replacement of Zr with Nb, would lead to more bonding M–M and M–Ni interactions, which are the only interactions with a significant contribution at the Fermi level. It turns out that the M–Ni interactions would be optimized at vec $= 48\ e^-$, which can formally be reached with a replacement of every second Zr with Nb. At that vec (Fermi level ca. -9.45 eV) not all bonding M–M states are yet filled. From these points of view, a "ZrNbNiP," crystallizing in the Hf_2NiP type, should be a stable compound.

Much has been written about the differences between metal-rich Zr and Hf compounds. Due to the larger extension of the 5*d* orbitals, Hf, compared to Zr, should prefer to form structures with more metal–metal contacts. Another reason for this trend is the higher contribution of *s* and *p* states in case of Hf (bcc-Hf: 1.5; bcc-Zr: 1.3), which are responsible for the long-range order, corresponding to the ideas of Brewer (24). Accordingly, HfNiP crystallizes in a structure with more M–M interaction than ZrNiP (Co_2Si type vs Ni_2In type) (25). In the isotypic $M_2M'P$ compounds, however, the Zr–Zr bonds possess higher MOPs than the corresponding Hf–Hf bonds, but lower Pauling bond orders (i.e., total PBO(Zr–Zr) = 1.40 per Zr atom in Zr_2CoP, and total PBO(Hf–Hf) = 1.51 per Hf atom in Hf_2CoP). Assuming that the Mulliken overlap populations provide a more reasonable evaluation of bond strengths, the Zr compounds show more M–M bonding than the Hf compounds. Also, the MOPs are higher for the Zr–P bonds, whereas the MOPs for the Zr–M' are slightly smaller than for the Hf–M' bonds. Apparently, the lower lying Zr *d* states are more filled than the Hf *d* states, leading to less oxidized Zr atoms, and in turn to a lower remaining electron density at the iron-group-metal atoms in the case of the Zr phosphides. Because of the sharp separation between the metal and nonmetal states, the differences between the ionization potentials of Zr and Hf are less important for binary phosphides and chalcogenides, which explains the occurrence of the different trends.

ACKNOWLEDGMENTS

H.K. thanks the DFG for the financial support of this work. The Ames Laboratory is operated by Iowa State University (ISU) for the US Department of Energy (DOE) under Contract W-7405-Eng-82 and is part of the Institute for Physical Research and Technology (IPRT) consortium of fundamental and applied research centers.

REFERENCES

1. R. L. Abdon and T. Hughbanks, *J. Am. Chem. Soc.* **117,** 10,035 (1995).
2. R. L. Abdon and T. Hughbanks, *Chem. Mater.* **6,** 424 (1994).
3. B. Harbrecht, *Z. Kristallogr.* **182,** 118 (1988).
4. B. Harbrecht and H. F. Franzen, *J. Less-Common Met.* **113,** 349 (1985).
5. B. Harbrecht, *J. Less-Common Met.* **124,** 125 (1986).
6. B. Harbrecht, *J. Less-Common Met.* **141,** 59 (1988).
7. M. Conrad and B. Harbrecht, *J. Alloys Compd.* **197,** 57 (1993).
8. H. Kleinke and H. F. Franzen, *Inorg. Chem.* **35,** 5272 (1996).
9. H. Kleinke and H. F. Franzen, *J. Alloys Compd.* **238,** 68 (1996).
10. H. Kleinke and H. F. Franzen, *Chem. Mater.* **9,** 1030 (1997).
11. H. Kleinke, *J. Alloys Compd.* [In press].
12. C. Wang and T. Hughbanks, *Inorg. Chem.* **35,** 6987–6994 (1996).
13. H. Kleinke and H. F. Franzen, *J. Alloys Compd.* [In press].
14. R. M. van Essen and K. H. J. Buschow, *J. Less-Common Met.* **64,** 277 (1979).
15. H. Kleinke and H. F. Franzen, *Angew. Chem. Int. Ed. Engl.* **36,** 513 (1997).
16. L. Pauling, "The Nature of the Chemical Bond," 3rd ed., Cornell Univ. Press, Ithaca, NY, 1948.
17. R. Hoffmann, *J. Chem. Phys.* **39,** 1397 (1963).
18. M.-H. Whangbo and R. Hoffmann, *J. Am. Chem. Soc.* **100,** 6093 (1978).
19. P.-J. Ahlzén and S. Rundqvist, *Z. Kristallogr.* **189,** 149 (1989).
20. H. Kleinke and H. F. Franzen, *Angew. Chem. Int. Ed. Engl.* **35,** 1934 (1996).
21. H. Kleinke. [unpublished research].
22. E. Clementi and C. Roetti, *At. Data and Nucl. Data Tables* **14,** 177 (1974).
23. T. Hughbanks, G. Rosenthal, and J. D. Corbett, *J. Am. Chem. Soc.* **110,** 1511 (1988).
24. L. Brewer, *in* "Alloying" (L. Walter, M. R. Jackson, and C. T. Sims, Eds.), Chap. 1, ASM International, Metal Park, OH, 1988.
25. H. Kleinke and H. F. Franzen, *Z. Anorg. Allg. Chem.* **622,** 1893 (1996).